Monthly Notices of the ROYAL ASTRONOMICAL SOCIETY

MNRAS **450,** 794–806 (2015) doi:10.1093/mnras/stv541

An 8-mm diameter fibre robot positioner for massive spectroscopy surveys

N. Fahim,[1] F. Prada,[2,3,4★] J. P. Kneib,[5,6] G. Glez-de-Rivera,[1] P. Hörler,[7] J. Sánchez,[4] M. Azzaro,[4] S. Becerril,[4] H. Bleuler,[7] M. Bouri,[7] J. Castaño,[8] J. Garrido,[1] D. Gillet,[9] C. Gómez,[2] M. A. Gómez,[10] A. González-Arroyo,[2,11] L. Jenni,[7] L. Makarem,[9] G. Yepes,[11] X. Arrillaga,[12] M. A. Carrera,[12] R. Diego,[12] M. Charif,[13] M. Hug[14] and C. Lachat[14]

[1]*Grupo de Investigación HCTLab, Escuela Politécnica Superior, Universidad Autónoma de Madrid, E-28049 Madrid, Spain*
[2]*Instituto de Física Teórica, (IFT, UAM/CSIC), Universidad Autónoma de Madrid, Cantoblanco, E-28049 Madrid, Spain*
[3]*Campus of International Excellence UAM+CSIC, Cantoblanco, E-28049 Madrid, Spain*
[4]*Instituto de Astrofísica de Andalucía (CSIC), Glorieta de la Astronomía, E-18080 Granada, Spain*
[5]*Laboratoire d'Astrophysique, Ecole Polytechnique Fédérale de Lausanne, Observatoire de Sauverny, CH-1290 Versoix, Switzerland*
[6]*Aix Marseille Université, CNRS, Laboratoire d'Astrophysique de Marseille, UMR 7326, F-13388 Marseille, France*
[7]*Laboratory of Robotic Systems (LSRO), Ecole Polytechnique Fédérale de Lausanne (EPFL), CH-1015 Lausanne, Switzerland*
[8]*Grupo de Electrónica y Semiconductores, UAM, E-28049 Madrid, Spain*
[9]*Coordination and Interaction Systems Group (REACT), School of Engineering, Ecole Polytechnique Fédérale de Lausanne (EPFL), CH-1015 Lausanne, Switzerland*
[10]*Escuela Técnica Superior de Ingenieros Aeronáuticos (ETSIA), Universidad Politécnica de Madrid, E-28049 Madrid, Spain*
[11]*Departamento de Física Teórica, Universidad Autónoma de Madrid, Cantoblanco, 28049 Madrid, Spain*
[12]*AVS (Added Value Solutions), Elgoibar, Gipuzkoa, E-20870 Elgoibar, Spain*
[13]*FAULHABER, Miniature Drive Systems, CH-6980 Croglio, Switzerland*
[14]*MPS Micro Precision Systems AG, PO Box 8361, CH-2500 Biel/Bienne, Switzerland*

Accepted 2015 February 25. Received 2015 February 2; in original form 2014 December 11

ABSTRACT

Massive spectroscopic survey are becoming trendy in astrophysics and cosmology, as they can address new fundamental knowledge such as understanding the formation of the Milky Way and probing the nature of the mysterious dark energy. To enable massive spectroscopic surveys, new technology has been developed to place thousands of optical fibres at a given position on a focal plane. This technology needs to be: (1) accurate, with micrometer positional accuracy; (2) fast to minimize overhead; (3) robust to minimize failure; and (4) low cost. In this paper, we present the development, properties, and performance of a new single 8-mm in diameter fibre positioner robot, using two 4-mm DC-brushless gearmotors, that allows us to achieve accuracies up to 0.07 arcsec (5 μm). This device has been developed in the context of the Dark Energy Spectroscopic Instrument.[1]

Key words: instrumentation: spectrographs – techniques: spectroscopic – surveys – large-scale structure of Universe.

1 INTRODUCTION

The recent Sloan Digital Sky Survey (SDSS) measurements of the baryonic acoustic oscillation peak in the distribution of galaxies (Eisenstein et al. 2005; Anderson et al. 2012) and in the Lyα forest of distant quasars (Delubac et al. 2015) are drawing new and important constraints on the cosmological world model. These successful measurements are paving the way for even more massive spectroscopic surveys that will improve significantly the number of targeted object in order to derive more stringent constraints on the cosmological world model with a particular focus on the characterization of the nature of dark energy – or at least its equation of state.

However, to enable such massive survey, new technology is needed to increase significantly the multiplexing capabilities of multi-object spectrograph on 4–8 m class telescopes. There are two main types of multi-object instruments: multislit spectrographs and fibre-fed spectrograph. Both offer advantages and disadvantages, but the most versatile type for object collection is the fibre-fed

★ E-mail: f.prada@csic.es

[1] This development was conducted by a Spanish–Swiss (ES-CH) team led by the Instituto de Física Teórica (IFT, UAM-CSIC) and the Laboratoire d'Astrophysique (EPFL), in collaboration with the Added Value Solutions (AVS) company in Spain and the Faulhaber group (MPS and FAULHABER-MINIMOTOR) in Switzerland.

approach. For all the fibre-fed spectrographs, the key issue to solve is the accurate positioning of the many optical fibres at the location of the targeted objects (star, galaxy or quasar) at a given sky position. For each sky position, the placement of the fibres is different. Therefore, the fibre positioning system has to be capable to adjust the position of fibres to the new targeted positions within a short amount of time (ideally faster than the detector readout time – typically less than one minute; or if done in parallel of the actual observation faster than the integration time). Different strategies have been used in previous instruments (e.g. see Smith et al. 2004 for a general review, or Haynes 2006 for a review on positioner technology): (1) for the SDSS spectroscopy surveys, fibres are placed by hand on a set of cartridges that are prepared during day time; (2) for the Anglo-Australian Telescope spectrograph, each fibre is sequentially picked and placed at its targeted position on a plate by a robotic system, while in parallel another plate is being observed ensuring a good duty cycle; (3) for the Large Sky Area Multi-Object Fibre Spectroscopic Telescope (Zhang & Qi 2008) and the *Subaru*/Fibre Multi-Object Spectrograph (Moore, Gillingham & Saunders 2002), an array of positioners places all the fibres simultaneously at the targeted positions, using back-illumination of the fibres. Such concept is the most versatile, as targets can be decided just before observations and the reconfiguration time is extremely short (typically less than one minute).

The new massive spectroscopy projects are almost all adopting the array of positioners as their fibre positioning system, we can list: Super Ifu Deployable Experiment (SIDE; Azzaro et al. 2010), Prime Focus Spectrograph/Subaru Measurement of Images and Redshifts[2] with the COBRA (Fisher et al. 2009) fibre positioner, 4-metre Multi-Object Spectroscopic Telescope,[3] Multi-Object Optical and Near-infrared Spectrograph,[4] and Dark Energy Spectroscopic Instrument[5] (DESI; Silber et al. 2012; and this work). These experiments will obtain optical/IR spectra for millions of galaxies, quasars and stars.

In this context, the group led by FP, in collaboration with the company AVS in Spain, has a long heritage and a valuable experience on developing precision fibre positioning mechanisms. Thanks to this partnership, it has built a 29 mm-pitch fibre positioner for the 10 m-Gran Telescopio de Canarias (GTC) telescope in the context of the SIDE instrument proposal (Prada et al. 2008), whose (R&D) expertise has allowed AVS to build the Multi-Espectrógrafo en GTC de Alta Resolución para Astronomía fibre positioner (Gil de Paz et al. 2014). We also developed a 12 mm-pitch $\theta - \phi$ fibre positioner competing prototype for Big Baryon Oscillation Spectroscopic Survey (BigBOSS; Fahim et al. 2013) that deliver excellent performance results, as presented in several BigBOSS/DESI collaboration meetings. This device, built late 2012 by AVS in partnership with the Instituto de Astrfísica de Andalucía (IAA-CSIC) and the Escuela Politécnica Superior (EPS-UAM), uses 6-mm geared stepper motors. The $\theta - \phi$ nomenclature is referred to the motion followed by the fibre positioner to place the fibre head through two angular degrees of freedom. This philosophy has been used in all the prototypes built by our collaboration, as that for SIDE at GTC and the previous BigBOSS prototype.

To go beyond the above development and reach a smaller size device of ∼8 mm diameter (meeting the latest DES requirements), we have worked on a new concept based on a Spanish–Swiss collaboration led by the Universidad Autónoma de Madrid (UAM) and the École polytechnique fédérale de Lausanne (EPFL) and including the following companies: AVS in Spain and the FAULHABER group (MPS and FAULHABER-MINIMOTOR) in Switzerland. The extended Spanish–Swiss group (hereafter ES-CH) has collaborated to design and manufacture a 10.4 mm-pitch fibre positioner based on the DESI science and technical requirements. The main objective was to reduce the size of the device, improve its mechanical robustness, but keeping the excellent performances of previously developed fibre positioners. The result of this project is presented in this paper, which describes the fibre positioner concept design, and show the performance results of the present ES-CH 10.4-pitch fibre positioner.

We organize the paper as follows. In Section 2, we describe the fibre positioner focal plane environment. The mechanical requirements are described in Section 3 and the fibre positioner concept design is described in Section 4. In Section 5, we present the properties and performance of the 4-mm DC-brushless gearmotors used in the fibre positioner. Performance and test results of the fibre positioner are discussed in Section 6. We conclude in Section 7.

2 THE CONTEXT OF THE NEW FIBRE POSITIONER

2.1 The DESI project

The Dark Energy Spectroscopic Instrument (DESI) project (Schlegel & Ghiorso 2008; Schlegel et al. 2011) aim to develop a new massive spectroscopy instrument to probe the nature of dark energy. This project funded largely by the US Department of Energy will use the NOAO 4-metre Mayall Telescope (Kitt Peak, Arizona, USA) on which will be mounted a fibre-fed spectrograph system.

2.2 The focal plane array

Mounted at the new prime focus optical structure (see Fig. 1), an array of 5000 fibre positioners (following the $\theta - \phi$ philosophy) will

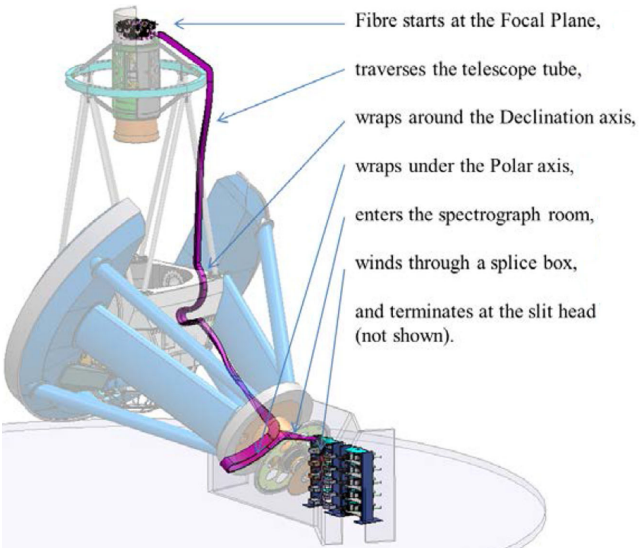

Figure 1. Routing of the fibre cable from the DESI prime focus optical structure at the NOAO 4-metre Mayall telescope, which contains the focal plane with the fibre positioner array (Image credit: DESI).

[2] http://sumire.ipmu.jp/en/2652
[3] http://www.4most.eu/
[4] http://www.roe.ac.uk/ciras/MOONS/VLT-MOONS.html
[5] http://desi.lbl.gov/

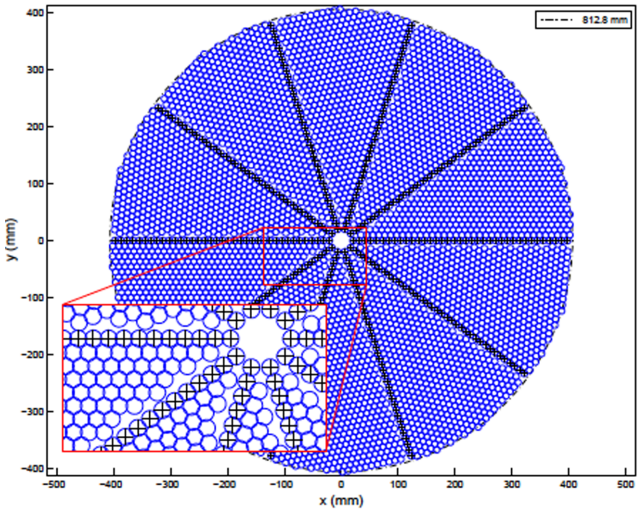

Figure 2. DESI focal plate layout. The focal plate is made of 10 petals; each will host 507 fibre positioners. The bottom-left panel shows a front zoom view of the focal plate petals mounted on the Integration Ring with some additional support. The blue rings represent the patrol disc of each fibre positioner, in other words, the area where each positioner can place its fibre head. The crossed rings represent the areas with no fibre positioners due to the layout of the focal plate.

be installed on a curved focal plate (2). This system will be able to control individually the position of 5000 optical fibres with an accuracy better than 0.07 arcsec (5 μm).

Each positioner can place a fibre at any location over a disc which will be called *patrol disc*. Adjacent patrol discs overlap so that most the positions on the focal plane can be reached by at least one fibre positioner. Of course, some parts of the focal plane can be reached by more than one fibre positioner, leading to the possibility of collisions between the arms of adjacent fibre positioner. To avoid this collisions, moving in parallel and in minimum time, we have developed a motion-planning algorithm for fibre positioners based on a novel decentralized navigation function (Makarem et al. 2014). The functionality and performance of this algorithm is described in Section 4.4.

To ensure the micro-metric placing of all the positioners in the focal plane, and to adapt the fibre to the optical curved field, a sectored focal plate has been developed (see Fig. 2). This structure is divided into 10 sections called petals, that contain the fibre positioners holes and a number of fiducial fibres used to calibrate the metrology of the entire system.

The position tolerances required by the fibre positioners for the fibre tips to be consistent with the aspheric focal surface of the instrument are ensured by manufacturing and tuning during the assembly phase. The focal plate is made of 10 petals, each of them being consistent through manufacturing tolerances with the focal surface geometry. With respect to the *XY* position tolerances of the fibre tips, the mechanical chain ensures the right position through tolerances stack-up starting from the focal plate petals up to fibre tips, passing through all the mechanical interfaces applicable to the positioner itself. The fact is that the *XY* positioning tolerances are in the range of what is achievable by manufacturing.

Concerning the *Z* position of the fibre tip, this tolerance produces defocus so it is highly critical. With regard to this, the applicable interfaces on the focal plate reproduce the aspheric geometry of the focal surface. Nevertheless, additional tuning is necessary in the interface between the fibre tip and the positioner in order to set

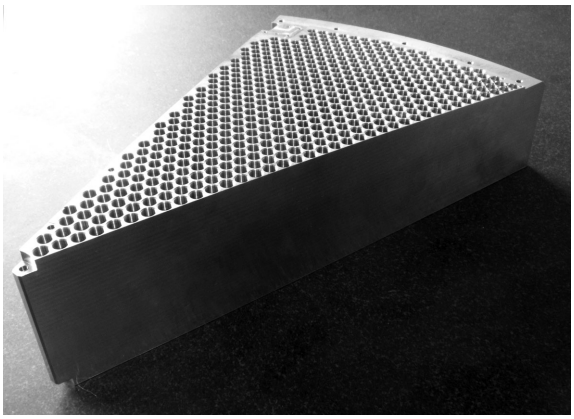

Figure 3. An individual petal, containing 507 fibre positioner holes. 10 of these petals will conform the entire DESI focal plate structure (Image credit: IAC).

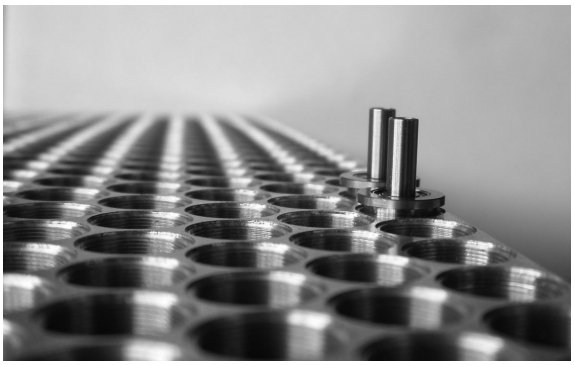

Figure 4. Detail of two dummy fibre positioners installed in two holes (Image credit: IAC).

the right *Z* location of it w.r.t. the focal surface. This means that the positioner will need an ancillary tool to tune the position of the fibre tip in *Z* direction.

Figs 3 and 4 shows one petal of this structure as built by the IAC in collaboration with the Lawrence Berkeley National Laboratory (LBNL), the IAA-CSIC and the IFT.

In order to find out the proper way to maximize the accuracy of the whole system, different interfaces to place the fibre positioner into the focal plate have been tested.

(1) Taped chassis of the positioner directly threaded on the petals threaded hole: this allows for a relatively large fine-pitch thread on the plates bulk.

(2) Extended chassis on the interface area to enable insertion of the two M2 screws directly on the petals plate: this means a high amount of small threads to be done on the plates bulk.

(3) Similar chassis to option 2, but based on magnets so no critical threads are implemented on the petals bulk: this was discarded for reliability reasons.

Finally, option 1 was implemented on our petal prototype; and manufacturing was successful and no wrong threads came up.

Table 1 shows the main parameters of the manufactured focal plate.

This array of fibre positioners offers many advantages. First of all, the reconfiguration times between two observing configurations are extremely short. The fibre positioners move in parallel to all the 5000 fibre following anticollision trajectories. The trajectories

Table 1. Focal plate main parameters.

Item	Value
Z position error of holes spotface	±0.21 arcsec (15 μmm)
XY position error on lateral position of holes	±0.42 arcsec (30 μmm)
Angular tolerance on holes orientation	±0.°02

are computed off-line following the avoidance collision algorithm. Therefore, the reconfiguration time of the fibre array is minimized (all the 5000 fibres are positioned in less than 45 s), optimizing the sky observation periods. In practice, each fibre positioner is controlled by a dedicated control hardware attached to the device. This philosophy provides an extremely robust, scalable and easy to maintain system, allowing us to control each fibre positioner individually, as well as any hypothetical failures of each fibre positioner (motor faults, collision errors, hardware failures, mechanic problems, etc.).

Although our team has worked on all the fibre positioner and focal plate aspects, in this paper we will focus on the description of one individual fibre positioner, describing its main characteristics, and reporting the most relevant performance results on positioning accuracy, reconfiguration times, mechanical advantages, as well as providing the results of the characterization of the adopted 4-mm DC-brushless FAULHABER motors. A future work will be devoted to the focal plate and will be published somewhere else.

3 MECHANICAL REQUIREMENTS

We list in Table 2 the most relevant requirements of the DESI fibre positioner. This paper focuses on the most critical aspects related to the position errors, which affect directly the position accuracy of the fibre within its patrol disc. The *XY* maximal error, the *XY* rms error, the *Z* maximal error and the angular tilt are the main values qualifying the position accuracy. Nevertheless, other important parameters are also discussed, in particular the power consumption, which can impact the signal-to-noise ratio if important temperature gradient are created, producing turbulent air flows near the focal plate.

Z position errors of the fibre tip produce a de-focus error which translates into a large spot not fitting the fibre's core, so a loss of energy is produced. Angular tilt errors lead to a focal ratio degradation (FRD) at the fibre's exit, with the optical performance being downgraded.

Table 2. Fiber positioner basic requirements.

Item	Value
Packing pattern geometry	Circular
Distance between fibre positioner centres (pitch)	10.4 mm
Patrol zone outer radius	6 mm
Robot diameter	8 mm
rms *XY* error	<0.07 arcsec (5 μm)
Max *XY* error	<0.14 arcsec (10 μm)
Z max defocus error	<0.09 arcsec (6.4 μm)
Max angular tilt	±0.°1
Max reconfiguration time	20 s
Power while active	1.204 W
Power while sleep	0.2 mW
Fibre bend radius	>50 mm
Operational temperature range	−10°+30°C
Mass of the fibre positioner	50 g
Lifetime	10 yr

The DESI robot is a tailored version of our previous BigBOSS prototype. In this respect, we are assuming that the life expectations for the present prototype will satisfy the DESI requirements. For the BigBOSS prototype, we executed more than 1000 h of tests (i.e. 180 000 movements) without any loss of accuracy.

We list below the different elements that can affect the fibre positioner accuracy.

(1) Size of the fibre positioner parts: the size of the parts is not exactly what is defined in the design (due to errors at the production level, or due to temperature variation). These differences induces an error in the position of the fibre. The most critical parts are the lengths of the two fibre positioner arms.

(2) Assembly imperfections: the dimensions of the assembled fibre positioner can also differ from what is defined in the design due to assembly imperfections (misalignment of parts for gluing, or unevenly tightened screws). The most critical assembly criterion is the alignment of the two rotation axes.

(3) Motion transmission irregularities: mechanical imperfections of the gears involved in the motion transmission can create irregularities in some areas of the fibre positioner patrol disc.

(4) Focal plate accuracy errors: such errors may be introduced by the focal plate hole-placing design or production. An angular deviation of the housing's axis produces tilt error and the *Z* position error of a spotface produces *Z* error.

Depending on the nature of these errors, we can distinguish those that can be compensated through software algorithms and those that cannot be solved. In the case of the DESI project, the fibre positioning system benefits from a fibre-view camera that can measure the position of each fibre (back-illuminated) after each movement. In this way, the main pointing algorithm executes sequentially an established number of iterations studying after each one the error between the real actual position and the theoretical target. Thus, the *XY* errors due to (1), (2) and (4) can be compensated with the corrections provided by the fibre-view camera system. However, *Z* errors, tilt errors and the *XY* error due to (3) cannot be solved with this method.

4 THE FIBRE POSITIONER CONCEPT DESIGN

The main purpose of the individual fibre positioner discussed in this paper is to place a fibre head into a specific patrol disc area of the focal plate with extremely high accuracy. This fact has forced us to design a robust robotic system, with really small dimensions based on a very small control electronics, where high-performance algorithms are embedded. The design developed is based on a message processor system. Thus, arrays with information will flow between the central computer and each fibre positioner, through a communication tree (see Fig. 5). The commands sent by the central computer will be processed in each individual fibre positioner and will represent the main inputs for the control algorithms. These algorithms will perform the placing of the fibre with high accuracy and small time requirements, thus they will perform the movements in close-loop, reporting the real position and the velocity in real time. This information will be sent to the central computer, and will represent the main inputs of the collision avoidance routines that will prevent the whole system of positioners of eventual critical failures (see Section 4.4). In the next sections, we present the main concept, properties and performance of a single fibre positioner.

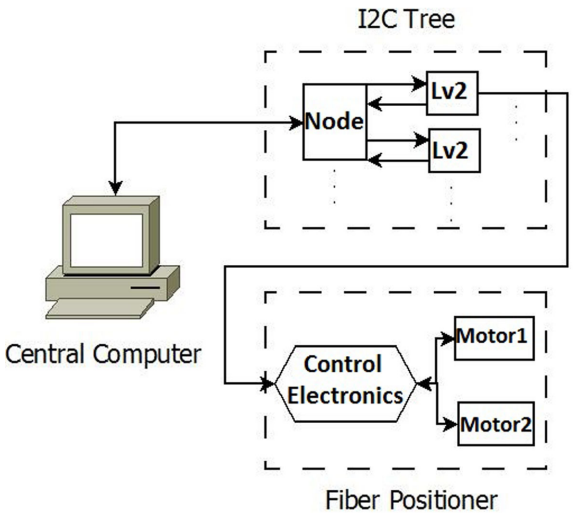

Figure 5. Control scheme for a single fibre positioner. Here, it is possible to note the bidirectional information flux between the control electronics of each robot and the central computer, through a two-level I^2C tree.

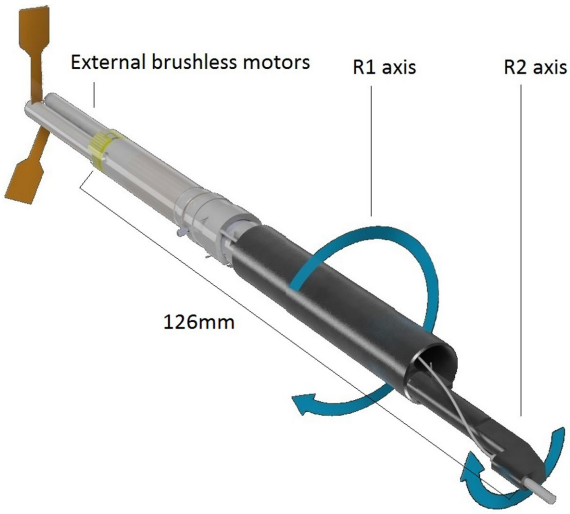

Figure 6. The new ES-CH fibre positioner. This prototype has a diameter of 8 mm and 165-mm long aluminium body (including motors), it is driven by two 4-mm DC-brushless gearmotors and makes the placing of the fibre tip through two angular degrees of freedom (i.e. rotations $R1$ and $R2$).

4.1 The mechanical design

The basic mechanical design of the fibre positioner was developed by the company AVS in collaboration with the IAA-CSIC (see Fig. 6). Two prototypes were built by MPS taking into account a critical optimization for serial massive production.

The mechanical concept of the DESI 10.4 mm-pitch fibre positioner presented in this paper is based on two coupled rotations, one nested into the other. The rotation over the main axis is called $R1$ ([0°–360°]), which, in turn, houses $R2$ ([0°–180°]). $R2$ is a rotation-nested off-axis in the $R1$ mechanism. By the combination of $R1$ and $R2$, a grid of positions within the patrol disc is provided. Fig. 7 shows this kinematic concept.

The present concept based on fixed $R1$, $R2$ motors leads to the fact that an $R1$ motion induces a motion in $R2$, even without running the $R2$ motor. So, in order to avoid that, the induced gearing ratio has to be compensated by $R2$. If the fibre tip has to be moved by $\delta R1$ and $\delta R2$ to reach a final position, then $R2$ has to move $\delta R2+(\delta R1/2.181\,818...)$, where the latter figure corresponds to the induced ratio. This compensated $R2$ movement has been called $RR2$ and is the main real position where the robot is moved for this axis.

All the ($R1$, $R2$) to ($R1$, $RR2$) transformations are done inside the fibre positioner control electronics. The fibre positioner accepts Cartesian (X,Y) coordinates or their own native coordinates ($R1$, $R2$), both coordinates system referred to its centre. To do that, each fibre positioner needs to know ($L1$, $L2$), where $L1$ and $L2$ are the lengths of the $R1$ and $R2$ arms. The fibre positioner centre and ($L1$, $L2$) are calculated with the help of the fibre-view camera.

The ES-CH fibre positioner includes the following main mechanical features.

(1) Pre-loaded transmission: unlike other fibre positioners, both axes involved in the ES-CH prototype are pre-loaded, generating more robust movements. The spring pre-load are used to minimize the gauge at the last stages of the gearbox, and the mechanism that this axis moves. It is due to the non-zero backlash gearbox used. It is based on a tensed spring with force less than the force used to move the mechanism.

(2) Hard stops for both $R1$ and $R2$: this prevents damage to the optical fibre in case of incidental run-out of the motors.

(3) Customized motor gearbox: decreased amount of parts to make the link with the main rotation axis, which implies an improved reliability of the device. This also leads to a lower cost of the fibre positioner.

(4) External motor architecture: the architecture followed in this fibre positioner presents both motors outside the chassis of the robot. On the one hand, this configuration increases the heat dissipation. On the other, it eliminates the electric wires all the way inside the positioner, thereby the twists of wires in moving sequences are minimized, and the life of the fibre positioner is extended.

On the other hand, the optical fibre is attached to the ferrule at the arm tip, it makes an helicoidal spline up to a coaxial hole, and goes straight up to the exit by the rear side (see Fig. 7). The minimal radius of curvature of the fibre along this path is 60 mm, so the present requirement given in Table 2 is fulfilled.

Finally, after the evaluation of several driver technologies, a 4-mm DC-brushless technology motor with hall-sensing control and integrated magnetic encoder, combined with a planetary gear-head, have been selected to ensure a reliable motion and precise accuracy. All necessary components were provided by FAULHABER-MINIMOTOR.

To fit the requirements of the fibre positioner in terms of dimensions, a ‘watch design and manufacturing technology’ have been considered to miniaturize the mechanical parts such stator, rotor,

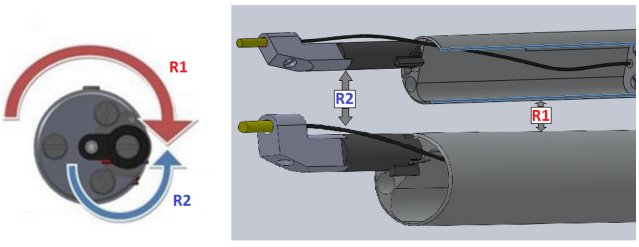

Figure 7. Left: frontal view of the ES-CH positioner. This image shows the kinematic concept of the positioner, where it is possible to see the movements of each axis (clockwise movement of the axis $R1$ and CCW movement of the axis $R2$). Right: fibre path in the ES-CH fibre positioner. In this image, it is possible to see, in a proper way, the two axes involved in the movement.

Table 3. Main characteristics of the Faulhaber 4-mm gearmotor.

Dimensions	
Diameter:	4 mm
Overall length:	34 mm
Performance	
Motor speed:	30 000 rpm @ 3.3 V
Output torque of the motor:	0.0108 mNm
Sensor:	6 pulses per rotation.
Gear ratio:	1024:1
Output torque of the gearmotor:	10 mNm

bearing, gears, shaft, etc. To ensure the accuracy of the systems and quality control, all components were manufactured with automatic computer numerical control (CNC) machines in-house at MPS. Table 3 shows the main characteristics of the motors.

Attending to the algorithms used to modulate the control signals for each motor, it is possible to generate up to 128 'steps' per rotation. In this way, the pulses generated by the sensors installed in each motor could be used in two ways. On the one hand, they could be used as a way to measure each step (up to six steps per rotation) in a low-resolution configuration. On the other, they could be used just to provide a closed-loop input to ensure a good movement for each axis and to avoid mechanical failures. This configuration allows us to achieve the best resolution, and considering the gearbox ratio, it is possible to achieve up to 0.001 arcsec step^{-1} (0.1 μm step^{-1}).

4.2 Control electronics

In order to move the two motors involved in the fibre positioner, and optimizing its performance, a basic electronics has been developed. This electronics will be placed inside the chassis of the fibre positioner. On the one hand, the components that conform the control electronics have been chosen following ultralow power consumption requirements; this characteristic allows us to minimize the thermal noise in the focal plane. On the other hand, all electronic components have to respect the volume constraints required by the board dimensions.

Fig. 8 shows the overall control electronics block diagram. The main component of the system is a 32-bit micro-controller, in charge of receiving commands from the top communication nodes, processing them and managing information flowing into the fibre positioner. This component will receive data through a fast I^{2}C bus up to 100 MHz, and will control with high accuracy the position of each motor through a full mosfet-based bridge system. The real position of each motor will be provided to the micro-controller, thanks to a magnetic encoder system embedded in each motor. This information

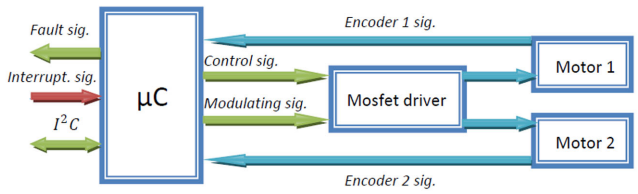

Figure 8. Overall block diagram for the control electronics. On the one hand, here it is possible to note the closed-loop architecture formed by the micro-controller command line and the sensors feedback signals. On the other, it is possible to see two feeding signals implicated in the modulation process that drive both motors through a high speed mosfet H-bridge.

will allow the micro-processor to modulate in real time the velocity of each motor, accomplishing the time constraints demanded by the Master system in order to follow the collision avoidance algorithm. On the other hand, this information will allow the system to know the existence of real movements and registering each time the existence of movement errors (hard motor fault, arrival to a physical zero, etc).

To optimize the consumption of the electronics, the micro-controller can run in two modes, i.e. Active and Sleep. The first one is used to process data, to monitor constants and to position the robot, whereas the second one is used in waiting command periods, reducing consumption to a minimum when not required. This feature is managed by an interrupt line that allows the Master software to manipulate directly the consumption state of each fibre positioner.

All the gearboxes with a high reduction ratio like those used in the DESI positioner show an intrinsic irreversibility, due to the difficulty to be moved in reverse mode. Then, the motor axis is not affected by the out gearbox force (included the pre-load spring), and there is no motor-axis position waiting. Thus, it is important to highlight that the motors involved in the fibre positioner do not lose steps in absence of current. Then, it is not necessary to feed them in sleep periods, this reduces the current consumption of the whole system, and minimizes the heat dissipation in the focal plane.

Finally, the motor control algorithms involved in our control electronics allow us to manipulate in real time the current that will flow though each motor, configuring directly the torque that the fibre positioner will use to move the fibre. This feature allows us to prevent some no movement motor errors caused by mechanics stress. To accomplish this goal, the magnetic encoder system will be used to check the existence of real movements and a windowed torque in case of the existence of this kind of errors.

Tables 4 and 5 show the main performance characteristics of the developed control electronic board.

It is important to highlight that the reconfiguration time of the fibre positioners is a main variable that allows us to maximize the number of spectra taken in an observation night. This parameter is defined as the time that the fibre positioner takes to move the fibre head between two points (i.e. targets). In this way, the control electronics developed for our prototype allows us to move the fibre positioner from end-to-end of the patrol disc in 30 s, whereas the total time taken to execute up to three iterations of the correction algorithm is 45 s (see Section 6). This last period includes the time

Table 4. ES-CH fibre positioner electronic characteristics.

Characteristic	Value
Power supply	3.3 v
Electrical power	Motor on: 600 mW Receiving command: 79.2 mW Sleeping: 0.66 μW
Connector pin	1+3.3 V 2 ground 3 SDA 4 SCL 5 Fail/OTB program
Mobile cables inside the positioner	No
Temperature housekeeping Stop error sensed	Yes Hall sensors detect bad stop condition

Table 5. ES-CH fibre positioner low-level software characteristics.

Characteristics	Value
Sleep motor	Yes
Sleep micro-controller	Yes
XY to *R*1–*R*2 bidirectional transformations	Yes
OTB programmable	Yes
Error management	If motor is blocked, then stop positioner and send an error

required to get the images, to process them in order to measure the error and to move the fibre positioner to the correct place. However, this reconfiguration time does not have a major importance in this moment for this prototyping phase (see Section 7).

4.3 Communication solution

We adopted a wired solution for the communications of the DESI fibre positioners. Following this scenario, all placement orders, configuration messages and alert advices will be sent from superior communication nodes to each fibre positioner through a fast plus I^2C bus achieving transfer rates up to 3.4 Mbps. This serial communication solution will route all the data packets from the master computer to all the fibre positioners through two router level modules. These modules will allow the distribution of the targets on sectors, respecting the maximum capacitance charges. This protocol allows us to link per unit and distributing the overall system workload.

On the other hand, in order to avoid the relevant bottle neck in the first router level, this link is replaced by an Ethernet connection that allows data transferences up to 1000 Mbps. Making a standard interface between the master computer and the first I^2C components, this structure allows different load distributions in order to respect the focal plate structure. Fig. 9 shows the overall communication proposal for DESI. This proposal allows the master computer to link with all the fibre positioners distributing the workload among the three router levels. On the other hand, it shows the time taken by the communication system to route one position message (3 bytes) to the whole system.

Finally, continuing with a low power consumption philosophy in order to minimize the thermal noise in the focal plane, this architecture has been designed selecting ultralow power consumption devices. Achieving power consumption levels up to 500 mW at 3.3 V for all branches pending of each level-1 nodes.

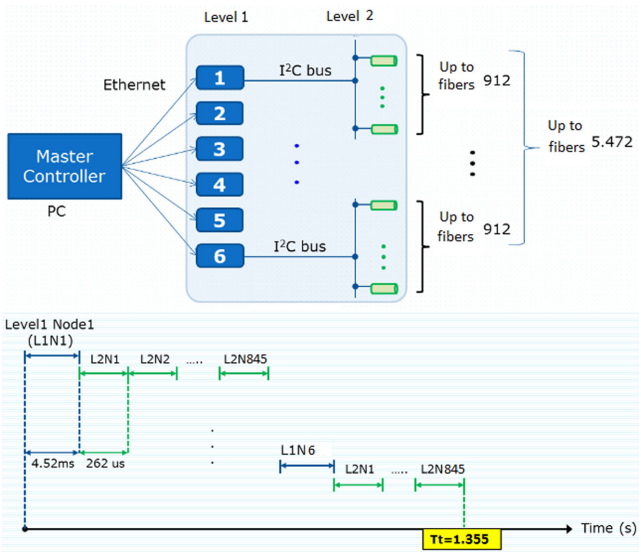

Figure 9. Top: overall communication architecture based on a two-level fast I^2C plus Ethernet tree. Bottom: timing simulation example. Here, it is possible to note that the whole sending process is completed in 1.355 s.

4.4 Collision avoidance algorithm

To get the most efficient scientific results from the planned survey, the 5000 fibre positioners need to move the fibre ends in parallel. As they share workspace, the most direct trajectories are prone to collision that could damage the fibre positioners and certainly have a serious impact on the survey operation.

As the first step, we have developed a visual simulation environment for the whole 5000 fibre positioners for testing and validation of target assignment (see Morales et al. 2012), motion planning and collision avoidance algorithms (see Fig. 10).

Then, we have provided a motion-planning algorithm for motors. The goal is to move in parallel and in minimum time all fibre positioners that are initially packed at a focal plane. The main challenges are ensuring collision avoidance and minimizing reconfiguration time.

Our proposed motion-planning framework for DESI is based on a novel decentralized navigation function. The navigation function

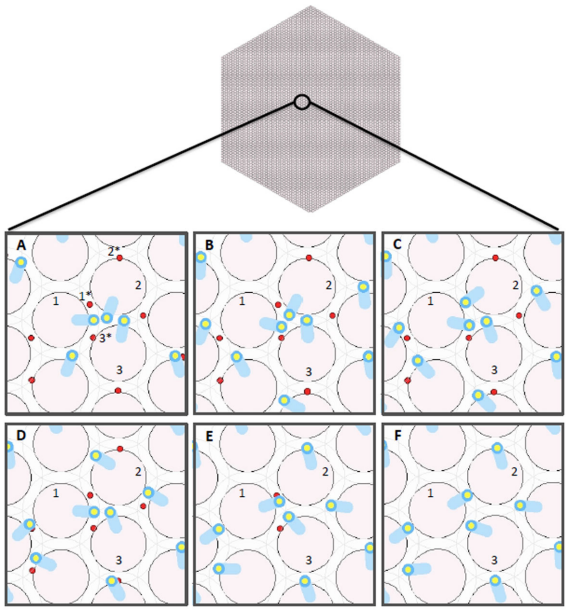

Figure 10. Simulation environment for 5000 fibre positioners and a zoom on the motion of three fibre positioners. The six boxes (A to F) show six snapshots of the simulation. 1*, 2* and 3* are, respectively, the target positions for fibre positioner 1, 2 and 3. These three fibre positioners are engaged in a local conflict in which fibre positioner 1 needs to make space for fibre positioner 2 to pass. Fibre positioner 2 cannot make room for fibre positioner 1 because fibre positioner 3 is blocking the way. Fibre positioner 3 needs to pass both fibre positioners to reach its target point. The small operation from fibre positioner 1 moves this fibre positioner farther from its target point but it makes room for the fibre positioner 2 to pass safely. When fibre positioner 2 clears the way, fibre positioner 1 starts moving towards its target point and this gives a safe way to the fibre positioner 3.

takes into account the configuration of fibre positioners as well as the fibre positioner constraints. An important aspect of our design is that we provided proof of convergence and collision avoidance. Decentralization results in linear complexity for the motion planning as well as independence of motion duration with respect to the number of fibre positioners. Therefore, the coordination method is scalable for large-scale spectrograph fibre positioners like DESI. The short in-motion duration of fibre positioners, approximately 2.5 s in DESI, will thus allow the time dedicated for observation to be maximized. Upon the preparation of the control board and fibre positioner prototypes, the designed trajectories will be tested in a close loop with the motors. The velocity profiles corresponding to the configuration presented in Fig. 10 and more detailed information can be found in (Makarem et al. 2014).

5 4-MM DIAMETER DC-BRUSHLESS MOTORS PERFORMANCE

In order to ensure that the motors meet the expected specifications in terms of accuracy, repeatability, and power consumption, three different tests have been developed. The first two tests have been developed on all the motors, letting us to know the main characteristics for all of them, and the last one just with two motors in order to characterize an overall proprietary.

5.1 Backlash and repeatability

To study the performance of the DC motors, a small mirror is mounted on the output shaft and a laser is pointed on the mirror (see Fig. 11). The reflected laser beam illuminates a spot on a wall. The position of the spot is related to the angle of the output shaft by $x = 2\alpha d$, where x is the position of the laser spot on the wall in millimetres, α is the angular position of the output shaft in radians and d is the distance between the mirror and the wall. In our case $d = 7000$ mm.

The backlash and repeatability are measured according to the following procedure.

(1) Move +X steps, then do −X steps.
(2) Measure position of the output shaft at position 0.
(3) Move −X steps, then do +X steps.
(4) Measure position of the output shaft at position 0.
(5) Go to 1.

The steps used in the procedure are one increment of the Hall sensor which corresponds to 60° on the motor shaft and translates to 0.°059 on the output shaft of the reduction gears. The measuring unit of the angle of the output shaft is 1 mm on the wall which corresponds to 0.°004.

The measurements at point 2 represent the position of the output shaft when coming from one side while the measurements at point 4 represent its position when coming from the other side. In both measurements, the position of the motor is the same, but the backlash interferes differently from the two sides. The difference between the measurements at points 2 and 4 represents the backlash in the reduction gears. The deviation within the measurements at point 2 represents the repeatability of positioning. The same applies for the measurements at point 4.

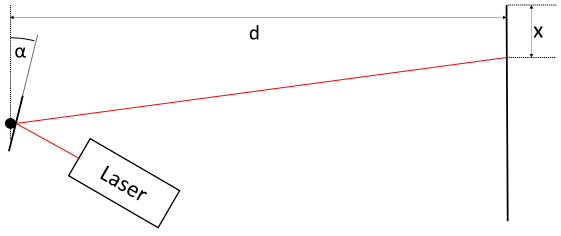

Figure 11. Schematic view of the measurement set-up, used to study the backlash and the accuracy of the motors adopted in the ES-CH positioner.

Table 6. Repeatability and backlash results (deg) of the six motors tested at 1000 rpm.

Device	Repeatability −	Repeatability +	Backlash
Motor 1	0076	0288	0043
Motor 2	0229	0161	−0,006
Motor 3	0136	0034	0741
Motor 4	0212	0212	0928
Motor 5	0042	0042	3151
Motor 6	0424	0068	0430

Table 7. Repeatability (deg) in terms of standard deviation of the six motors tested at 1000 rpm.

Device	Repeatability −	Repeatability +
Motor 1	0.028 399	0.0876 16
Motor 2	0.083 601	0.0646 67
Motor 3	0.045 81	0.0126 88
Motor 4	0.077 491	0.0799 67
Motor 5	0.015 86	0.0183 54
Motor 6	0.161 461	0.0249 87

Tables 6 and 7 summarizes the results of our measurements on six custom-made motors moving 500 step at the speed of 1000 rpm. The 'repeatability −' respectively 'repeatability +' are the standard deviations of the measurements at point 2 respectively 4 in the procedure. The backlash is the difference between the averages of the measurements at points 2 and 4 in the procedure. The first observation is that Motor 5 has a relatively large backlash. This is probably due to an imperfection or dust in the reduction gears. The backlash of the other motors stays in an acceptable range. All the motors show satisfactory repeatability according to the technical requirements.

It is important to note at this point that these measurements include only the motor and gearhead and that the DESI ES-CH fibre positioner includes pre-loaded springs to minimize backlash in both rotations. However, this results are important in order to understand the influence of each piece in the final accuracy result.

Finally, it is important that the backlash of the gearbox itself is small enough to be cleared out by the pre-loaded spring.

5.2 Power consumption

In these series of measurements, the motors are driven at a constant speed in both directions in a closed loop using the digital hall sensors. An amperemeter measures the electric current passing through the power bridge that drives the three phases of the motor.

Fig. 12 shows the current consumption of Motors 1, 3, 4 and 5 in clockwise and counter-clockwise (CCW) rotations.

The first observation is that Motor 5 has an unexpected non-linear behaviour. Its current consumption has a maximum at about

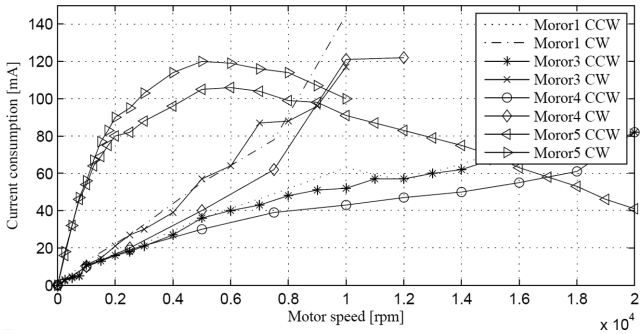

Figure 12. No-load current consumption of Motors 1, 3, 4 and 5.

5000 rpm. Then, it decreases towards the maximum speed. This can be explained by the manufacturing defect which could be also responsible for the big backlash and seems to have less influence at higher speeds.

The second observation is that the other motors rotating clockwise have a consumption about twice as high as rotating CCW. In addition, the maximum speed of clockwise rotation is about half of the CCW maximum speed. This is due to the fact that the angular offset between the motor and the hall sensor is optimized for CCW rotation. In the future, we will set the offset as a function of turning direction and expect the same consumption in both directions. In case of using encoders instead of hall sensors to provide feedback, the consumption can be reduced.

The current consumption of two motors plus the electronics will easily meet the requirements of maximum heat dissipation. The current measured here times the operating voltage (3.3 V) gives the power consumed by one motor including dissipation in the power bridge. With the requirement of max 1.2 W of heat dissipation per fibre positioner, the requirement is 363 mA per fibre positioner. In the worst case (both motors at full speed), our fibre positioner consumes only 160 mA. As it is mentioned in this article, the motors used in this application do not lose steps in absence of feeding, thus, the power consumption of both motors in sleep periods is 0 W.

5.3 Current consumption control

Knowing the minimum torque that moves the motors is needed not only for minimizing the consumption of the whole system but also to have total control of the fibre positioner movement. Therefore, we conducted a test for measuring the minimum torque for the two of the motors (Motor 1 and Motor 2).

It is worth mentioning that the electronics developed specifically for the fibre positioner are able to control the maximum current that will pass through each motor (therefore, the torque given to each one), by modulating the control lines with a Pulse-Width Modulation (PWM) signal. Thus, the torque of each motor is proportional to the duty cycle of the modulating PWM signal.

In this test, the duty cycle of the modulating signal has been incremented from 1 per cent up to 50 per cent, measuring the current consumption while the movement of the motor is measured by the Hall sensor.

Table 8 and Fig. 13 show the results achieved in this test. The figure shows the consumption of the motors as function of the duty cycle. The duty cycle from which the motor starts a bad movement (vibrations) corresponds to the point where the consumption begins to decrease. The duty cycle from which the motor starts to move correctly is the point where the consumption starts to rise again. Looking at the consumption where the motor moves correctly, we can observe that it is linear and very similar for both motors. Thus, we can conclude that the minimum torque that we can apply to each motor in order to control them correctly is 32 per cent of the maximum.

Table 8. Characteristic behaviour patterns shown by both motors used in the tested prototype, when they are fed with low duty cycle ranges.

Motor	Starting (non-regular)	Fails	Starting (regular)
Motor 1	16	24–30	32
Motor 2	14	–	27

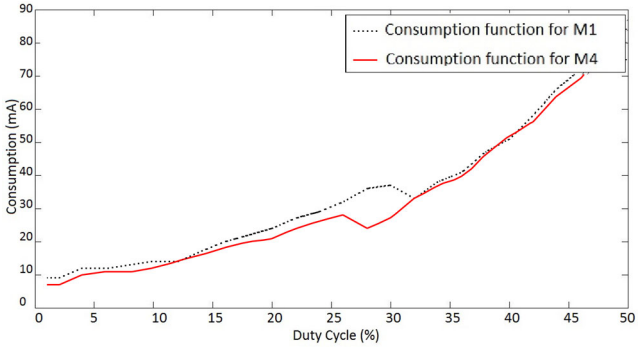

Figure 13. Current consumption for Motors 1 and 2 as a function of the duty-cycle of the feeding signals.

5.3.1 *Magnetic coupling*

The two motors involved in each fibre positioner are installed in parallel positions with a considerably short distance. Due to the magnetic principles that control this kind of motors, it is important to study the effect of the magnetic field of one motor on the movement of the other (inductive effects). In addition, the magnetic field could cause noise and distortions on the Hall sensor signals.

In order to study the relevance of magnetic effects in the motor performance, we have measured the emitted magnetic field of one motor in movement with an analogical Hall sensor, the electric induction in one disconnected motor winding and we studied the coupling between two running motors.

To prove the real magnetic coupling influence in the motor control, the two motors are moved the same number of steps, one after the other and the total number of rising edges of the magnetic encoder signal of each motor are compared. After a significant set of tests, it has been proven that there is no influence in the individual movement of the motors when they are in direct contact.

6 FIBRE POSITIONER TESTING SET-UP

A camera-based fibre view set-up has been used to characterize the performance of our fibre positioner. This set-up allow us to ensure that the DESI requirements listed in Table 2 are met in terms of accuracy, backlash and repeatability. The multi-iteration procedure for high-precision positioning has also been evaluated.

The optical set-up consists on a Santa Barbara CCD camera developed for astronomical applications (SBIG STF-8300), a multi-axis positioning stage holding the fibre positioner and a fixed fibre used as a reference. The camera is installed in front of the positioner, at a distance that allows us to see at the same time both fibres and

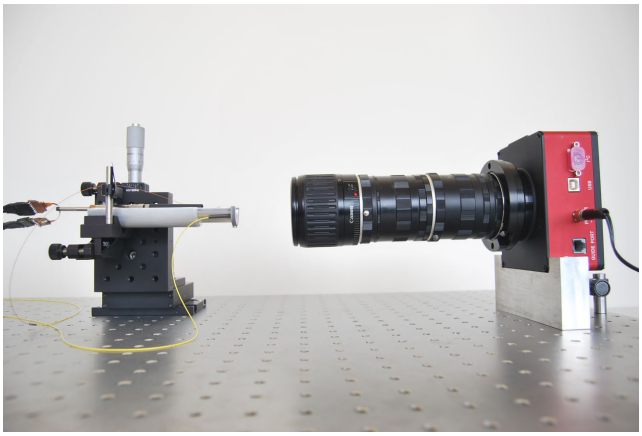

Figure 14. Lateral view of the optical set-up, used for the automation of the fibre positioner testing process.

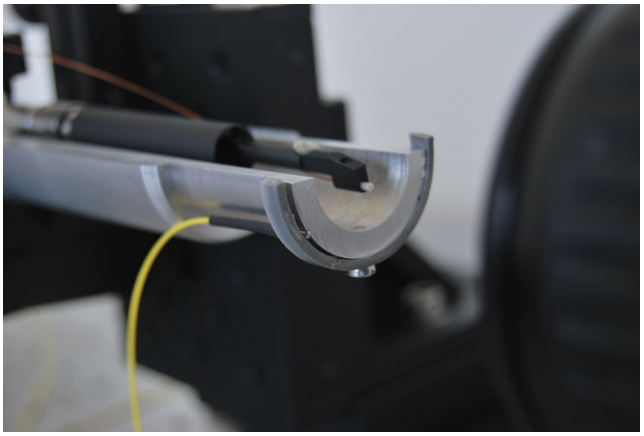

Figure 15. Reference fibre holder, used to obtain absolute position measurements.

the whole movement of the fibre positioner. In order to ensure the focusing of the plane, a short lens (Cannon 80-200) and two generic macro expanders (6.5 mm) have been used. To minimize the vibrations and guarantee the stability, all these components are mounted on an optical granite table and assembled using specific aluminium parts, manufactured in a CNC machine.

Fig. 14 shows a lateral view of the optical set-up with the fibre positioner placed in front of the camera. As shown in the figure, the CCD camera has been mounted with two macro expanders and a Cannon macro lens.

6.1 Accuracy measurements

The camera is connected to a PC where an automatic MATLAB routine developed by J. Silber at LBNL is executed. This routine communicates with the user interface of the fibre positioner, it sends a position target, waits for the end of the movement and takes a picture. After each shot, the routine extracts the distance between the fibre moved by the fibre positioner and a second optical fibre used as a reference.

It then computes the difference between the fibre position and the theoretical one, establishing this as the system accuracy. On the other hand, this system allows us to calibrate the fibre positioner at the beginning of each test, establishing the actuator centre, the real length of its arms ($L1$, $L2$) and configuring the allowed positions.

Fig. 15 shows the reference static fibre mounted in an aluminium piece built for this purpose.

The MATLAB program executed in this optical set-up emulates the main actions that the master computer of the DESI telescope will have to perform once the 5000 fibre positioners will be mounted on the focal plate. To maximize the accuracy, this routine executes a pre-established number of iterations, determining after each movement the error between the positioned fibre head and the static reference, using these data as the input of the next iteration in order to make the necessary corrections. The *XY* accuracy results obtained will be shown as the main representative performance data for the characterization of the ES-CH 8-mm fibre positioner.

7 RESULTS

The three main variables that characterize this kind of $\theta - \phi$ fibre positioner, are the repeatability, the accuracy and the mechanical hysteresis. These data ensure that the fibre positioner will place the fibre head at the same point in extremely different situations, minimizing the error between the theoretical target and the attained one.

In order to study the accuracy of the fibre positioner, a simple test has been developed. A set of position targets evenly distributed on a grid and filling the whole patrol area is defined. The master routine commands the fibre positioner to move successively on every target point executing five correction iterations for each evaluated position. The main purpose of this procedure consists on obtaining the maximum number of target positions with an absolute *XY* error less than 0.07 arcsec (5 μm) [value obtained with the previous 10-mm diameter prototype developed by the Spanish group for the former BigBOSS project (Fahim et al. 2013)].

Fig. 16 shows the results obtained with one of the fibre positioner prototypes. This figure presents the theoretical positions (blue crosses) and the achieved ones (red crosses). The second image in this figure shows the effect of the corrective iterations on the position accuracy. Here, it is possible to note the percentage of positions with an accuracy error less than a concrete value. Hence, it shows the efficiency of the corrective movements. This preliminary result shows that 80 per cent of the points can be reached with an absolute error less than 0.07 arcsec (5 μm) after five iterations of the corrective algorithm.

The results achieved with this test show a similar behaviour of the corrective movements than the accomplished with the BigBOSS prototype. Thus, it is possible to note that the maximum efficiency of the algorithm is shown in the first three iterations. Therefore, just three corrective movements will be necessary to place the fibre head in its final position.

These results have a significant relevance, because all of them have been obtained without running any hysteresis reduction algorithm (see below). In fact, all the results collected in Fig. 16 meet the requirements of the DESI project in terms of maximum absolute error, rms error and percentage of positions with less than 0.07 arcsec (5 μm) in absolute *XY* error.

Table 9 shows the data collected in these preliminary tests. It is possible to observe that the maximum absolute error after the fifth iteration is lower than 0.14 arcsec (10 μm) (maximum value allowed, see Table 2). On the other hand, it is important to highlight that the resulting rms error is less than 0.07 arcsec (5 μm) after the second iteration.

Finally, the minimum error values achieved after the execution of this test show that both the mechanics and the control electronics

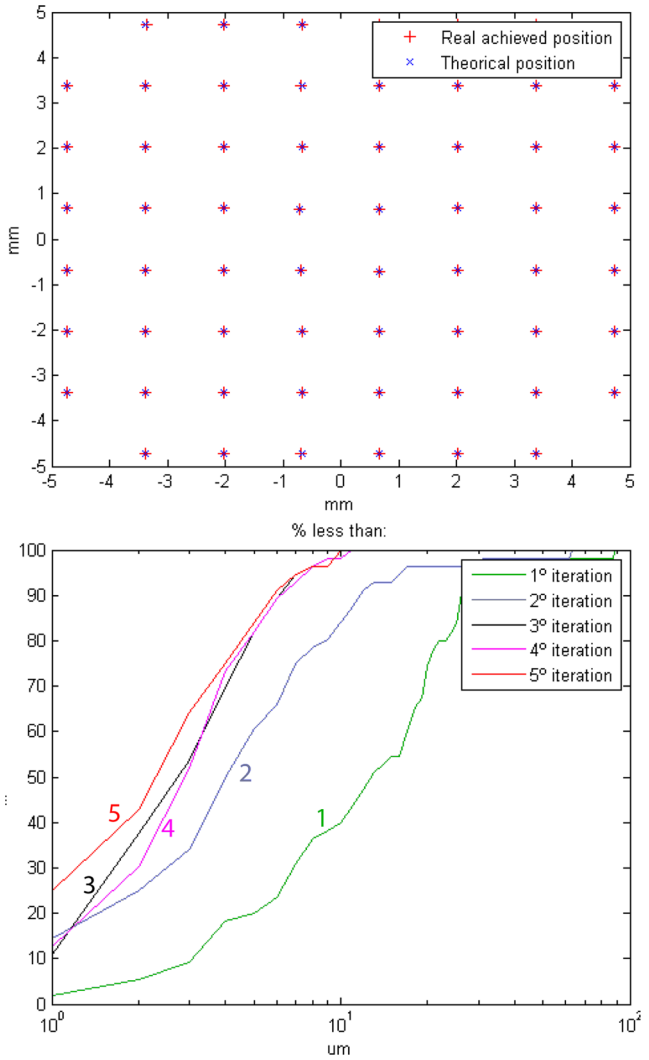

Figure 16. Top: visual results after the execution of a grid test through the optical set-up. Red crosses correspond to the achieved positions, and blue plus symbols correspond to the theoretical position. Bottom: cumulative distribution of the absolute *XY* error for the different iterations.

allow us to accomplish incredible accuracy results. Thus, nowadays it is working in the definition of specific backlash reduction algorithms that will allow us to increase the fibre positioner accuracy up to these values.

After the performance of extensive experiments, we can conclude that continuous execution of several grid tests, with a significant number of targets over the entire patrol disc, were enough to characterize the accuracy of our fibre positioner prototype. These tests were performed during several hours, letting us to evaluate the effects of the stress in both motors. On the other hand, after several entire nights running grid tests, we could note that there were no losses of steps. This evidence showed us the robustness of the close-loop algorithms, and the efficiency of the hall encoders embedded into each motor.

All tests described in this paper, and the results achieved through them, refer to a single prototype (one of the two manufactured up to date).

Table 9. Main accuracy results achieved after the execution of a complete grid test through the optical set-up.

	<5 μm (per cent)	<2 μm (per cent)	<1 μm (per cent)	rms (μm)	Max (μm)	Min (μm)
1 Mov.	1.8	0	0	138.1	342.2	3.4
1 Iter.	20.0	5.5	1.8	19.9	88.1	0.5
2 Iter.	60.7	25.0	14.3	11.1	62.6	0.4
3 Iter.	82.1	37.5	10.7	3.9	10.6	0.3
4 Iter.	82.1	30.4	12.5	3.8	10.4	0.5
5 Iter.	83.9	42.9	25.0	3.6	9.8	0.2

7.1 Backlash characterization

In this subsection, we aim to quantify the cumulative effect of the different transmission stages on the final positioning accuracy.

From the results obtained with the optical set-up, it was possible to characterize the internal mechanical response of the evaluated prototype. In particular, one of the most representative mechanical characteristic of this fibre positioner is the internal hysteresis. The position of the fibre depends on the movement of two motors. In this way, the backlash of each rotation axis depends on the direction of rotation of the motor, the amplitude of the displacement and the velocity profile. Thus, the positions achieved by the fibre positioner while trying to reach one target in the patrol disc will be different for every starting point.

Fig. 17 shows the results obtained while trying to move from one starting point (A) to a target point (B), and returning to the starting point. A characteristic mismatch can be seen between the points along the path from A to B and the points along the path from B to A.

In order to minimize this mechanical error, a software algorithm able to reduce up to 10 times this error was developed. To make it real, this algorithm forces the fibre positioner to move inside a preliminary backlash region (area that depends on the residual backlash of the positioner), before it reaches the target position. This action softens the internal mechanics before the final movement. It is important to note that the smaller the fibre positioner, the more difficult it will be to reduce this kind of mechanical errors due to the soft properties of the metals of these small sizes.

Fig. 18 shows the results of the test run shown in Fig. 17 after the implementation of the hysteresis reduction algorithm. In this figure, it is possible to see how the previous movements, done to soften the internal mechanics before the movement to each target, reduce drastically the system hysteresis. Hence, how the points recorded in the way from (A) to (B) and those recorded in the way from (B) to (A) are closer than before. In respect to the real movements

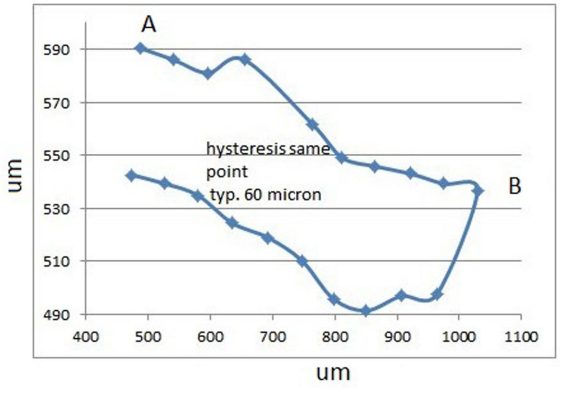

Figure 17. Characteristic hysteresis pattern in the *XY* plane (units are μm), due to the internal mechanical architecture.

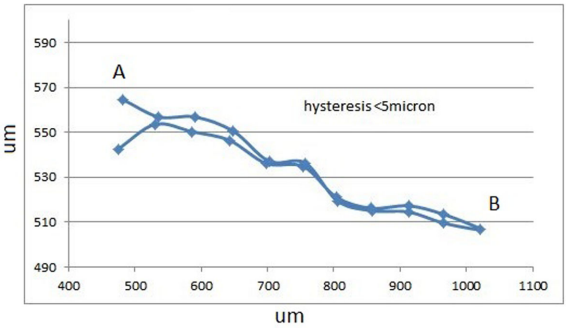

Figure 18. Hysteresis pattern after applying the hysteresis reduction algorithm.

that the positioner will perform in the focal plate, the reduction of the hysteresis will reduce the accuracy errors that depends on the direction of the rotation of each motor. With the expertise obtained with our prototype for the BigBOSS project, we can say that this represent an overall reduction of the errors measured in the whole patrol disc area.

The hysteresis errors depend only on the internal mechanic and physical behaviour, thus the algorithm developed to reduce them has a specific design for each fibre actuator and its particular characteristics.

Due to the reduced dimensions of the present design, the hysteresis properties of the internal mechanics presents different behaviours than our previous prototypes. Hence, nowadays, based on the results accomplished with the BigBOSS prototype, we hope to define the best parameters to adapt the hysteresis reduction algorithm to the DESI prototype, in order to increase the accuracy of the positioner.

7.2 Main results

The tests developed for the fibre positioner are based on an entire robot (fibre included) attached to an Alta-Azimuthal table inside a thermal chamber to simulate all the spatial orientations, and temperature conditions. All this has allowed us to know the toughness and the incredible resistance of the prototype, and has made possible the contention of all the results with the maximum accuracy. Thus,Table 10 summarizes the requirements for the DESI fibre positioner and the results obtained by our ES-CH prototype presented in this paper.

The main results that characterize the developed fibre positioner, are the rms and the Max *XY* error. These accuracy results have been obtained through the execution of several grid tests, under the conditions mentioned above.

Table 10. Required and achieved values.

Item	Required	Achieved
rms *XY* error	0.07 arcsec (5 μm)	0.05 arcsec (3.6 μm)
Max *XY* error	0.14 arcsec (10 μm)	0.138 arcsec (9.8 μm)
Z max defocus error	0.42 arcsec (30 μm)	0.09 arcsec (6.4 μm)
Max angular tilt	$\pm 0\overset{\circ}{.}1$	$\pm 0\overset{\circ}{.}058$
Max reconfiguration time	20 s	30 s
Power while active	<1.204 W	0.6 W
Power while sleep	<0.2 mW	0.66 μW
Fibre bend radius	>50 mm	70 mm
Mass of the fibre positioner	<50 g	30 g

The defocus and tilt tests, were developed for our previous BigBOSS fibre positioner prototype by Pat Jelinsky and JS at LBNL in 2013 March (Allington et al. 2013). We use an optical bench with a laser *XY* reference surface, in which it is installed the positioner with a ceramic flat piece attached to the optical fibre (the reference surface and the flat piece are parallel for all positioner positions). Thus, on the one hand, the defocus test consists in to measure the *Z* location or distance to the reference surface, as a function of the different positions of the positioner. The result is a peak-to-valley variation of 0.09 arcsec (6.4 μm) for all the actuator positions (after removing a *Z*-temperature deviation). On the other hand, the tilt test was done using the same set-up, but measuring the angle between the incident light and the returned light to the ceramic semimirror piece as a function of the positioner positions. The result was a maximum tilt of $0\overset{\circ}{.}06$, an average tilt of $0\overset{\circ}{.}035$ and an rms tilt of $0\overset{\circ}{.}019$.

The final consumption results place the positioner into the required specifications, respecting the thermal dissipation boundaries. The results obtained during active periods have been achieved while the positioner places a fibre head at maximum velocity and torque (maximum duty-cycle of the motor feeding signal), considering the control electronics consumption in this period. On the same way, the consumption obtained during the sleep mode has been measured when the fibre positioner is waiting for a new placing command. In this period, both motors are stopped, and just the micro-controller is demanding current to maintain its sleep mode. Hence, the power consumption is negligible.

According to the route of all the fibres across the telescope (40 m), the most important stress point for the fibre is the positioner. Thus, the cable declination pivot, and the cable polar pivot are not important because their radii of curvature are very conservatives (>300 mm). The studies of Jeremy Allington-Smith and Graham Murray (Durham University) (Allington et al. 2013) gave us some ideas to keep in mind so that we do not stress the fibre: (i) the bad condition is an increment in the FRD due to scattering caused by the micro-bends in the fibres; (ii) the injection angle is important too, a bad angle increases the FRD; (iii) the twist of the fibre inside the actuator increases the FRD. In this way, to minimize all the effects exposed above, we need a small curvature radius and fibre positioning perpendicular at the input light beam. The minimum bend radius permitted to the fibre in the actuator is given by the Gloges power flow equation (Gloge 1972), the result for an *f*/4.8 input ray gives that integrated rms change in curvature is what matters, not the curvature itself, then to prevent bad FRD effects an $R > 1000r$ must be a limit (R = radius of curvature, r = fibre radius). Thus, considering the actual 140 μm fibre, this implies a 70 mm bend radius. However, Grossan, Meijer, Smoot (UCB SSL, Institute for Early Universe, Seoul) (Allington et al. 2013) noticed a serious problem when a fibre is twisted more than 360° in a 12-mm long cable. In this situation, the full width at half-maximum increases two times, and a temporal FRD memory effect appears between the baseline, twist and relax times. To avoid this effect, all the fibre across the positioner travels in a similar way than a straight line. Thus, in the fibre positioner the most important effect is the twist. To prevent it, the fibre is almost free in a path of around 200 mm long. However, in our prototype, this implies a total rotation of 540°, but we choose a medium attaching point, at which the rotation is around 270° (less than the boundary of 360°).

Finally, with these results, it is possible to notice that the reconfiguration time achieved by our fibre positioner prototype, at the moment, is higher than the required (see Table 10). As it has been showed in this paper, our main goal is to ensure the good accuracy

of the system and to study methodologies to improve it. Thus, the current reconfiguration times have been increased in order to minimize dynamical influences in the precision of the fibre positioner. However, both the control electronics and the mechanical properties of the robot allow us to reduce this value and eventually meeting the requirements. Nowadays, it is working in the definition of dynamical acceleration/deceleration curves to ensure good accuracy results at high speed.

8 CONCLUSIONS

We have presented here the development of a new ES-CH 8-mm fibre robot positioner that fulfils all the requirements of the DESI project. The main features of the mechanical design of our fibre positioner are: (i) the two motors are located at the bottom of the positioner and no electric wire circulate through the fibre positioner; (ii) the fibre path is relatively straight, ensuring minimal light loss.

We have also designed a control scheme to minimize the electronics consumption, maximizing the system accuracy and defining new command algorithms in order to avoid any hypothetical collisions between adjacent fibre positioners. On the other hand, failure alert techniques developed in the control electronics ensure the avoidance of mechanical critical failures, lengthening the whole system life and minimizing the need for maintenance.

Based on the different tests performed, we believe that our development has led to one of the most robust fibre positioner for massive spectroscopy instruments. The technology developed may possibly be adapted to other multifibre spectrograph projects.

ACKNOWLEDGEMENTS

We acknowledge support from the Spanish MICINNs Consolider-Ingenio 2010 Programme under grant MultiDark CSD2009-00064, HEPHACOS S2009/ESP-1473, and MINECO Centro de Excelencia Severo Ochoa Programme under grant SEV-2012-0249. We also thank the support from a CSIC-AVS contract through MICINN grant AYA2010-21231-C02-01, and CDTI grant IDC-20101033; and support from the Spanish MINECO research grants AYA2012-31101 and FPA2012-34694. JPK, PH and LM acknowledge support from the ERC advanced grant LIDA and from an SNF Interdisciplinary grant. We thank J. Silber and R. Bessuner at LBNL for helping to set up a replica of their testing optical bench set-up at EPS-UAM.

REFERENCES

Allington S. et al., 2013, Desi Collaboration Meeting. Available at: http://desi2013.lbl.gov/program.htm
Anderson L. et al., 2012, MNRAS, 427, 3435
Azzaro M., Becerril S., Vilar C., Arrillaga X., Sánchez J., Morales I., Carrera M. A., Prada F., 2010, Proc. SPIE, 7735, 773544
Delubac T. et al., 2015, A&A, 574, 59
Eisenstein D. J. et al., 2005, ApJ, 633, 560
Fahim N., Glez-de Rivera G., de Castro A., Garrido J., Sanchez J., Prada F., 2013, 28th Conference on Design of Circuits and Integrated Systems, San Sebastian, Spain
Fisher C., Braun D., Kaluzny J., Haran T., 2009, IEEE Aerospace Conference paper #1185, Version 5
Gil de Paz A. et al., 2014, Proc. SPIE, 9147, 91470O
Gloge D., 1972, Bell Syst. Tech. J., 51, 1767
Haynes R. et al., 2006, in Atad-Ettedgui E., Antebi J., Lemke D., eds, Proc. SPIE Conf. Ser. Vol. 6273, Optomechanical Technologies for Astronomy. SPIE, Bellingham
Makarem L., Kneib J.-P., Gillet D., Bleuler H., Bouri M., Jenni L., Prada F., Sanchez J., 2014, A&A, 566, A84
Moore A. M., Gillingham P. R., Saunders W., 2002, in Tyson J. A., Wolff S., eds, Proc. SPIE Conf. Ser. Vol. 4836, Survey and Other Telescope Technologies and Discoveries. SPIE, Bellingham, p. 299
Morales I., Montero-Dorta A. D., Azzaro M., Prada F., Sánchez J., Becerril S., 2012, MNRAS, 419, 1187
Prada F., Azzaro M., Rabaza O., Sánchez J., Ubierna M., 2008, in McLean I. S., Casali M. M., eds, Proc. SPIE Conf. Ser. Vol. 7014, Ground-based and Airborne Instrumentation for Astronomy II. SPIE, Bellingham, p. 70144F
Schlegel D., Ghiorso B., 2008, Proc. SPIE, 7018, 701850
Schlegel D. J. et al., 2011, preprint (arXiv:1106.1706)
Silber J. H. et al., 2012, in Navarro R., Cunningham C. R., Prieto E., eds, Proc. SPIE Conf. Ser. Vol. 8450, Modern Technologies in Space- and Ground-based Telescopes and Instrumentation II. SPIE, Bellingham, p. 845038
Smith G., Brzeski J., Miziarski S., Gillingham P. R., Moore A., McGrath A., 2004, Proc. SPIE, 5495, 348
Zhang Y., Qi Y., 2008, Proc. SPIE, 7019, 701928

This paper has been typeset from a TEX/LATEX file prepared by the author.